PCCP

Accepted Manuscript

ROYAL SOCIETY OF CHEMISTRY

www.rsc.org/pccp

Journal Name

ARTICLE

Effects of Amino Acid Sequence on Thermal Conduction through β-Sheet Crystals of Natural Silk Protein

Received 00th January 20xx,
Accepted 00th January 20xx

DOI: 10.1039/x0xx00000x

www.rsc.org/

Lin Zhang,[a] Zhitong Bai,[a] Heng Ban[a] and Ling Liu[a]

Recent experiments have discovered very different thermal conductivities between the spider silk and the silkworm silk. Decoding the molecular mechanisms underpinning the distinct thermal properties may guide the rational design of synthetic silk materials and other biomaterials for multifunctionality and tunable properties. However, such an understanding is lacking, mainly due to the complex structure and phonon physics associated with the silk materials. Here, using non-equilibrium molecular dynamics, we demonstrate that amino acid sequence plays a key role in the thermal conduction process through β-sheets, an essential building block of natural silks and a variety of other biomaterials. Three representative β-sheet types, i.e. poly-A, poly-(GA), and ploy-G, are shown to have distinct structural features and phonon dynamics leading to different thermal conductivities. Fundamental understanding of the sequence effects may stimulate the design and engineering of polymers and biopolymers for desired thermal properties.

Introduction

Natural silk materials produced by spiders and silkworms[1] have drawn considerable attention in the past couple of decades due to their extraordinary mechanical properties,[2, 3] biodegradability, and biocompatibility.[4, 5] These unique properties have enabled diverse applications of natural silk materials in making biomedical sutures[6] and implantable devices,[7] and in drug delivery as the drug carriers targeting cancer cells.[8, 9] Recently, these materials were made even more attractive for their thermal properties. The dragline silk made by *Nephila clavipes*, a golden orb-web spider, was measured to have a thermal conductivity of 1.2-151 $Wm^{-1}K^{-1}$, surpassing many materials.[10, 11] By contrast, the thermal conduction in silkworm silk is much less efficient. With thermal conductivities as low as 0.54 $Wm^{-1}K^{-1}$,[12] silkworm silk-based textiles have been used as thermal insulator for thousands of years.[13] From fundamental point of view, it is striking that the spider and silkworm silks (Figure 1*ab*), both spun by arthropods, have such distinct thermal conducting capabilities.

Structurally, both spider and silkworm silks are made of proteins rich in β-sheet, a protein secondary structure consisting of aligned polypeptide strands interlocked by hydrogen bonds. In these silk proteins, the abundant β-sheet crystals are embedded in a semi-amorphous matrix of 3_1 helices and β-turns (Figure 1*c*),[14] contributing significantly to the physical properties of the silk materials. For instance, our previous study has shown that the thermal conductivity of the poly-alanine (poly-A) β-sheet,[15] an essential building block of the *Nephila clavipes* spider silk, can be 1-2 orders of magnitude higher than that reported for other protein structures.[16] The main contributor to this phenomenon is the hydrogen bonding between the β-strands (i.e. the polypeptide strands) that form the β-sheets. As heat is carried by phonons in the β-sheet, the inter-strand hydrogen bonds blue-shift the frequencies of the low-frequency phonon modes, which further enhance thermal conduction.

Despite the progress, it remains unclear how heat is conducted differently in the β-sheets constituting the spider and silkworm silks. Structural biology has revealed that the β-sheets in different types of natural silk feature different amino acid sequences. For instance, the dragline silk from the *Nephila clavipes* spider has abundant poly-Alanine (poly-A) repeats (Figure 1*d*) while the cocoon silk from the *Bombyx mori* silkworm features poly-(Glycine-Alanine) [poly-(GA)] repeats (Figure 1*e*).[14, 17] Such a difference in the protein sequence has been found responsible for the distinct mechanical properties of different types of β-sheets.[18] Nevertheless, how thermal conduction is affected by the protein sequence is relatively unknown. Deciphering the correlation between the thermal properties and the protein sequence may improve our fundamental understanding of the nanoscale thermal transport phenomena in biomaterials. The results may further guide the design of synthetic silk materials[19, 20] to achieve tunable thermal properties with inherent biocompatibility, which is desired by many biomedical applications that demand high-performance thermal regulation. A word of caution though, is that β-sheet nanocrystals only account for ~30% of the residues in the *N. clavipes* dragline,[14, 21] and ~50% in the *B. mori* silk.[14, 22] The amorphous phase is also critical in determining the overall thermal properties of the silks. However, compared with β-sheets, the amorphous phase is typically associated with more phonon scattering and shorter mean free path of phonons leading to slower thermal conduction.[23] Therefore, this work focuses on the β-sheets which are the main thermal conductors in silks, aiming to reveal the effects of amino acid sequence on their intrinsic thermal conductivities.

To assist the understanding of the thermal transport process in β-sheets, it is helpful to draw an analogy between the protein β-sheets and other low-dimensional nanomaterials including nanotubes and nanowires, and search for similarities and distinctions in the thermal transport mechanisms. First, we note that all β-strands in the β-sheets (Figure 1*de*) feature numerous side chains/atoms (e.g. $-CH_3$ and -H) that are anchored to the backbone of the polypeptide chains

[a] Department of Mechanical and Aerospace Engineering, Utah State University, Logan, UT 84322, USA.

Electronic Supplementary Information (ESI) available: structural models, and identification of hydrogen bonds. See DOI: 10.1039/x0xx00000x

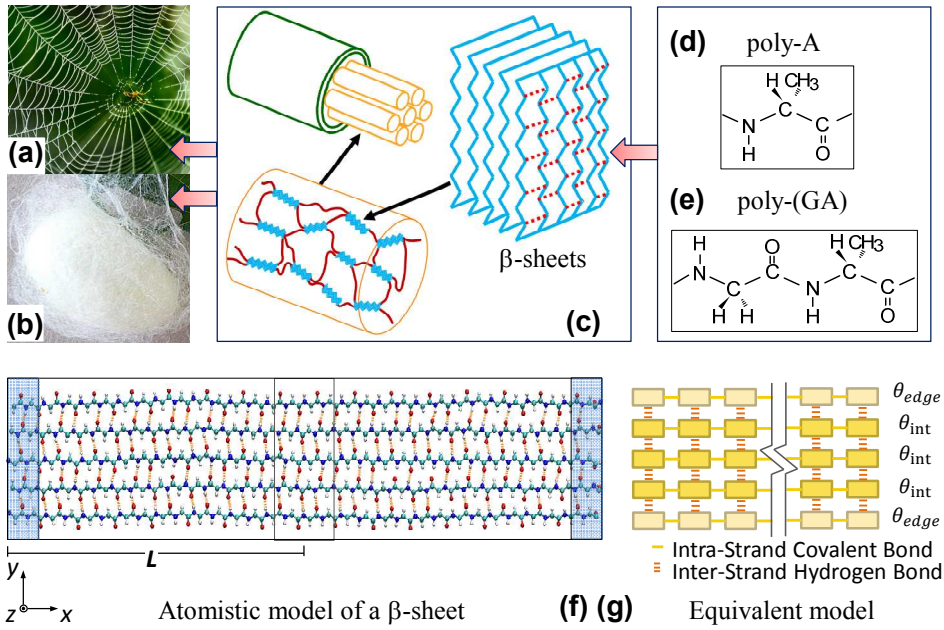

Figure 1. Natural silk from (a) the *Nephila clavipes* spider and (b) the *Bombyx mori* silkworm have a similar hierarchical structure in which the (c) β-sheet protein structure serves as an essential building block. In natural silk proteins, the β-sheets form numerous crystalline domains (blue) that are embedded in an amorphous matrix (red curves). Each of the β-sheets consists of multiple β-strands interlocked by hydrogen bonds (red dash lines). The β-sheets in different types of natural silk may have different amino acid sequences. For example, the β-sheets in the *Nephila clavipes* spider silk feature repeated (d) poly-A motifs, while those in the *Bombyx mori* silkworm silk are formed by repeated (e) poly-(GA) motifs. (f) To compute the thermal conductivity of a β-sheet, heat flow is generated from the "heat source" (red region) to the "heat sink" (blue region) by a velocity swapping algorism. *L* denotes the characteristic length of the model. (g) The β-sheet is analogous to a network of thermal resistors. Each strand is represented by a line of thermal resistors whose total resistance is denoted by θ_{edge} or θ_{int}, depending on the location of the strand.

(i.e. -N-C-C-). This is analogous to the carbon nanotubes functionalized by chemical attachments of alien molecules or atoms. Second, the poly-(GA) β-strand in Figure 1*e* is analogous to the superlattice nanowires that have alternating elements along the length direction. Previous studies have shown that: 1) carbon nanotubes functionalized by phenyl rings[24] and hydrogen atoms[25] have lower thermal conductivities than their pristine counterparts due to the reduced phonon mean free path; and 2) most superlattice nanowires have lower thermal conductivities than the nanowires of pure composition,[26] mainly due to the prominent phonon scattering at the material interfaces. It is hypothesized that the similar structural features dictate the thermal conduction process in β-sheets as well, while the detailed mechanisms are to be revealed.

Here we report a non-equilibrium molecular dynamics study of the thermal transport phenomena in three representative β-sheet types, i.e. poly-(GA), poly-A, and poly-G. The poly-(GA) β-sheet is abundant in the *Bombyx mori* silkworm silk, while the ploy-A β-sheet dominates in the *Nephila clavipes* spider silk. The poly-G β-sheet is a conceptual sequence for comparison. The analysis allows us to probe the fundamental physics underpinning the different thermal conductivities of natural silk materials. By systematically investigating the effects of sequence and structure, we will show in detail the phonon dynamics and molecular mechanisms associated with the thermal transport processes. The results will be further discussed in comparison with those reported earlier on the thermal conduction in synthetic low-dimensional materials. The conclusions may expand our understanding of the role of hydrogen bonds in facilitating thermal conduction in β-sheets, and guide the design of biomaterials for desired thermal properties.

Models and Methods

Full-atom atomistic models were constructed for the β-sheets with specific sequences and various sizes. We note that each β-sheet may exist in two different forms, i.e. the parallel and antiparallel configurations. This study is focused on the antiparallel β-sheets only, because they are more dominant in the *Nephila clavipes* dragline and *Bombyx mori* cocoon silks [17]. Each β-sheet model is composed of a specific number of β-strands that have the same characteristic length of 6.15 nm. The model is named as X*m*-*n*-1, where X indicates the repeated residues in the peptide, *m* is the total number of the repeats in a single β-strand, *n* is the number of β-strands in each layer, and "1" means that this study focuses on monolayer β-sheets. To eliminate phonon scattering with geometric boundaries, periodic boundary conditions were applied along all three directions. The unit cell was set to be large (40 nm) along the *y*- and *z*-directions to prevent periodic images of the β-sheet from interacting with each other in these directions. In all these models, about 70% hydrogen bonds form between the β-strands, which confirms that the structures are stable and appropriate for subsequent simulations (see details in ESI). It deserves mentioning that in this study, all β-sheets were placed in vacuum to focus on their intrinsic thermal conductivities. In real silk materials, however, there are several extrinsic factors that may affect the thermal conduction process, e.g. interaction with the amorphous phase and the surrounding water molecules. Between the two factors, water may have less influences due to its low presence in natural silks.[27, 28] The amorphous phase may scatter phonon transport in β-sheets and

change their thermal conductivities to some extent. However, we believe the interaction with the amorphous phase will not overturn the sequence effects to be revealed by this study.

The reverse non-equilibrium molecular dynamics method developed by Muller-Plathe[29] was employed to calculate the thermal conductivity. The method has been applied to many different material systems including polymers, nanotubes, nanowires, and liquids,[30] and has been shown to give consistent results as the equilibrium Green-Kubo method.[31] To apply the method, it is required that the system contains two copies of the β-sheet to be analyzed, i.e. the original model and an image, both physically connected and symmetric about their center along the direction of intended heat flow (*x*-direction in this study). The entire system was then divided into *N* slabs along the *x*-direction. A heat flux was numerically generated by continuously swapping the velocities of the "coldest" atoms (with the lowest kinetic energy) in the "heat source" slab and the "hottest" atoms (with the highest kinetic energy) in the "heat sink" slab (Figure 1*f*). Fourier's law was then employed to evaluate the thermal conductivity based on the heat flux generated in the system and the heat flux-induced thermal gradient. During this velocity-swap process, a virtual elastic collision model[32] was employed to ensure the conservation of both system energy and momentum equilibrium. The induced heat flux was evaluated by $J = \Delta E/2tA$, where t denotes the time interval between two swaps, ΔE is the averaged kinetic energy transferred per swap, A is the cross-sectional area of the material, and the coefficient "2" reflects the two symmetric heat transport paths from the hot slab to the cold slab. Finally by Fourier's law, thermal conductivity was calculated by $\kappa = -J / \frac{dT}{dx}$, where d$T$/d$x$ is the temperature gradient along the *x*-direction. Due to the symmetric nature of the system, the characteristic length, L, of the model equals to half the system length.

All simulations were performed using LAMMPS[33] with the CHARMM22 force field[34] to describe the interatomic interactions. Particle-particle particle-mesh method (PPPM) was adopted to address long range Coulomb's interactions with a root mean square accuracy of 10^{-4}. Nosé-Hoover thermostat was employed to maintain system temperature at desired values. Time step was set to be 1 fs. Prior to each simulation for obtaining thermal conductivity, the initial molecular structure was relaxed by minimization with the conjugate gradient method, followed by molecular dynamics equilibration at the temperature of 300 K for 5 ns. Then, a heat flux was induced by enabling the Muller-Plathe algorithm. The simulation was performed for 450 ns and only the last 400 ns was used to sample the temperature profile and heat flow. For all cases, no noticeable difference was identified between the thermal conductivities calculated using the 50 ns - 250 ns simulation results and those calculated using the 250 ns - 450 ns simulation results, indicating that the calculated thermal conductivities were stable with time. Moreover, to eliminate possible spurious global rotation of the molecule, global angular momentum was subtracted from the momentum of every atom at all steps. To avoid protein denaturation at high temperatures,[35] simulation parameters were optimized to ensure that the temperature difference between the hottest and coldest slabs in the system was 30±2 K.

In addition to the computation of thermal conductivity, phonon density of states (DOS) was also evaluated to further reveal the thermal transport mechanisms. Fourier transformation of the velocity autocorrelation function (VAF) was calculated for all/selected atoms following the equation $\rho(\omega) = \frac{1}{\sqrt{2\pi}} \int_0^{+\infty} e^{-i\omega t} \frac{\langle v(t) \cdot v(0) \rangle}{\langle v(0) \cdot v(0) \rangle} dt$ where $\rho(\omega)$ is the DOS with the angular frequency ω, $v(t)$ is atomic velocity, and <•> denotes an average over the selected atoms.

Results and Discussions

Figure 2*a* plots the computed thermal conductivities of all the β-sheets under investigation. To reveal the sequence and size effects, all β-sheets were built to have the same length of 16 residues, while the width was varied by changing the number of the β-strands. The results show prominent width effects. As the number of β-strands increases from 1 to 9, the thermal conductivity of the poly-(GA) β-sheet increases from 0.84 to 2.09 $Wm^{-1}K^{-1}$ (blue circles in Figure 2*a*). Additionally, it can be speculated that the thermal conductivity should converge to a certain value as the β-sheet becomes infinitely large. Similarly, the poly-G and poly-A β-sheets also give the same ascending trend. The thermal conductivity of the poly-A β-sheet increases from 1.85 to 4.30 $Wm^{-1}K^{-1}$ (black squares), while that of the poly-G β-sheet increases from 2.29 to 6.11 $Wm^{-1}K^{-1}$ (red diamonds). The size effects are attributed to the hydrogen bonds interlocking β-strands to form the β-sheets, which blue-shift the frequencies of the low-frequency phonon modes and facilitate thermal conduction. Similar hydrogen bond effects have been discovered in a-helices to enhance thermal diffusion.[36]

All of these results agree with a thermal resistance model developed in our previous work[15] which reveals that: 1) the thermal

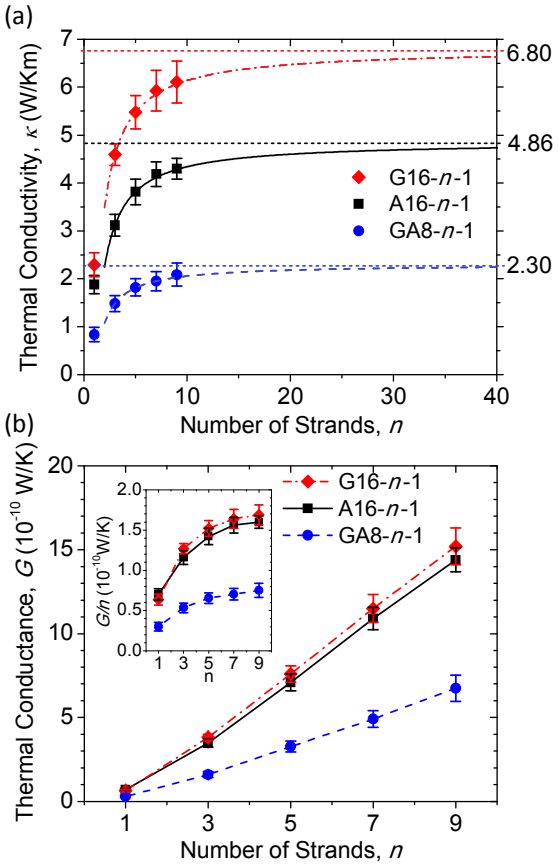

Figure 2. (a) Thermal conductivity and (b) thermal conductance versus the number of β-strands (*n*) for the poly-A, poly-G, and poly-(GA) β-sheets. The results in (a) are fitted by a thermal resistance model to predict the thermal conductivities of larger β-sheets. The inset in (b) plots the thermal conductance divided by the number of β-strands.

β-sheet	Thermal Conductivity (W/K·m) $n = 1$	$n > 2$	
	κ_{single}	κ_{edge}	κ_{int}
A16-*n*-1	1.85	2.25	4.86
GA8-*n*-1	0.84	1.07	2.30
G16-*n*-1	2.29	3.49	6.80

Table 1. Computed thermal conductivities of three standalone β-strands (κ_{single}), and the interior and edge β-strands in the corresponding β-sheets (κ_{int} and κ_{edge}).

conductivity of a β-sheet increases with the number of β-strands in the β-sheet (n); 2) the thermal conductivity of any β-strand in the β-sheet depends on the degree of hydrogen bonding; and 3) as n becomes infinitely large, the thermal conductivity of a monolayer β-sheet converges to that of an interior β-strand in the β-sheet. Figure 1*f* shows a poly-A β-sheet (A-16-5-1) that has five β-strands interlocked by hydrogen bonds. The thermal resistance model simplifies the β-sheet as a network of residues as shown in Figure 1*g*. The β-strands are further divided into two groups – edge strands and interior strands, with their thermal conductivities denoted by κ_{edge} and κ_{int}, respectively. The overall thermal conductivity of the β-sheet is derived as $\kappa = 2\kappa_{edge}/n + (n-2)\kappa_{int}/n$. Using the results in Figure 2*a*, κ_{edge} and κ_{int} of the poly-A, poly-G, and poly-(GA) β-sheets are evaluated and tabulated in Table 1. It is readily seen for all the three types of β-sheets, edge β-strands and interior β-strands have different thermal conductivities; κ_{int} is higher than κ_{edge}, and both of them are higher than κ_{single}, the thermal conductivity of a stand-alone β-strand of the same type. This is consistent with the fact that the interior β-strands are connected with more hydrogen bonds than the edge β-strands in a β-sheet, and a stand-alone β-strand has no hydrogen bond. Furthermore, the model also predicts increasing thermal conductivity with n, which agrees with the computational results in Figure 2*a*. As n keeps increasing, $\kappa_\infty = \kappa|_{n\to\infty} = \kappa_{int}$ gives the upper limit of the thermal conductivity.

The results in Figure 2*a* and Table 1 also show prominent effects of the amino acid sequence. At any particular width, the poly-G β-sheet gives the highest thermal conductivity among the three types of β-sheet under investigation, poly-A β-sheet the second, and poly-(GA) β-sheet the lowest. In terms of the upper limit of thermal conductivity (κ_∞), the poly-G β-sheet (G16-*n*-1) is approximately 40% higher than the poly-A β-sheet (A16-*n*-1) and 196% higher than the poly-(GA) β-sheet (GA8-*n*-1). In addition to affecting the thermal conduction in β-sheets where hydrogen bonds play a key role, the sequence of amino acids also influences the conduction of heat in standalone β-strands. As shown in Table 1, the thermal conductivity of the standalone GA8-1-1 β-strand is calculated to be the lowest, 55% lower than that of A16-1-1, and 63% lower than that of G16-1-1. The similar ranking between the standalone β-strands and the β-sheets implies that the sequence effects are inherent to proteins and not strongly influenced by hydrogen bonds.

These results are consistent with previous experimental measurements and provide clues for us to understand the varied thermal properties among different natural silks. As an essential building block of the *Nephila clavipes* spider silk protein, the poly-A β-sheet is shown by our computation to be a good thermal conductor, which contributes to the experimentally measured high thermal conductivity of the spider silk. Similarly, the low thermal conductivity of the *Bombyx mori* silkworm silk is partly attributable to the inefficient thermal conduction in poly-(GA) β-sheet. Furthermore, the computational results also provide a hint on the peptide design for engineering superior thermal-conducting biomaterials. Given the high thermal conductivities of the poly-A β-sheets, incorporating more poly-A motifs in the peptides may form β-sheets of better thermal conducting capabilities, thereby improving the thermal properties of the biomaterials. This is particularly pertinent to the design of synthetic silk materials in which amino acid sequence can be engineered following an optimized blueprint.

To reveal the mechanisms underlying the different thermal conductivities between the poly-A and poly-G β-sheets, we first convert the thermal conductivities into the thermal conductances. Thermal conductivity (κ) is the property of a material to conduct heat, while thermal conductance (G) is the property of a plate of particular length and cross section to conduct heat. They are correlated by $\kappa = L \cdot G / A$, where A is the cross-sectional area and L is the length of the plate. To calculate G for any β-sheet under investigation, we note that κ and L are readily available while A is lacking. The cross-sectional area of low-dimensional materials such as graphene and nanotubes have been studied for decades and there are many approaches available. In this study, the cross-sectional area of a β-sheet was evaluated based on a time- and spatial-averaging approach. As illustrated in Figure 3, a β-sheet under equilibrium was simulated for 1 ps, during which 1000 snapshots were stored. The position of a β-strand was quantified by averaging the coordinates of all backbone atoms constituting the strand over the 1000 snapshots. The cross-sectional area per stand (A_{strand}) was then calculated based on the area occupied by the β-strand on an averaging basis. In this way, A_{strand} was evaluated to be 25.46 Å^2 for the poly-A β-sheets, 21.46 Å^2 for the poly-(GA) β-sheets, and 17.08 Å^2 for the poly-G β-sheets.

Using the areas and thermal conductivities computed above, the thermal conductances of all β-sheets under investigation are calculated and plotted in Figure 2*b*. Similar with the thermal conductivity, the thermal conductance is also found to increase with the number of β-strands, which again, demonstrates that hydrogen bonding facilitates thermal transport in β-sheets. More importantly, it is striking to discover that the poly-G and poly-A β-sheets have very close thermal conductances despite their distinct thermal conductivities. In other words, the difference in sequence (i.e. poly-A versus poly-G) only affects the thermal conductivity significantly, while not changing the thermal conductance notably. Given $\kappa = L \cdot G / A$, the poly-G and poly-A β-sheets (with same L) have almost the same G, so $\kappa \sim 1/A$. That is, to tune the thermal conductivity of a β-sheet made with homogeneous amino acids, we

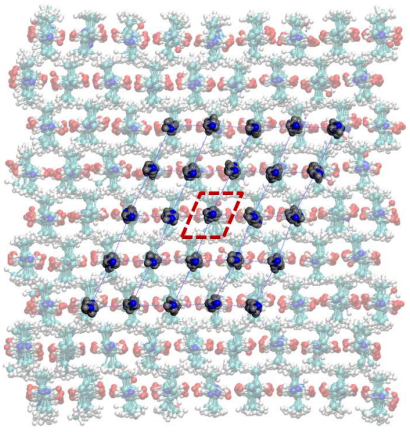

Figure 3. Evaluation of the cross-sectional area of a poly-A β-strand based on the equilibrium positions of the interior β-strands in a β-sheet.

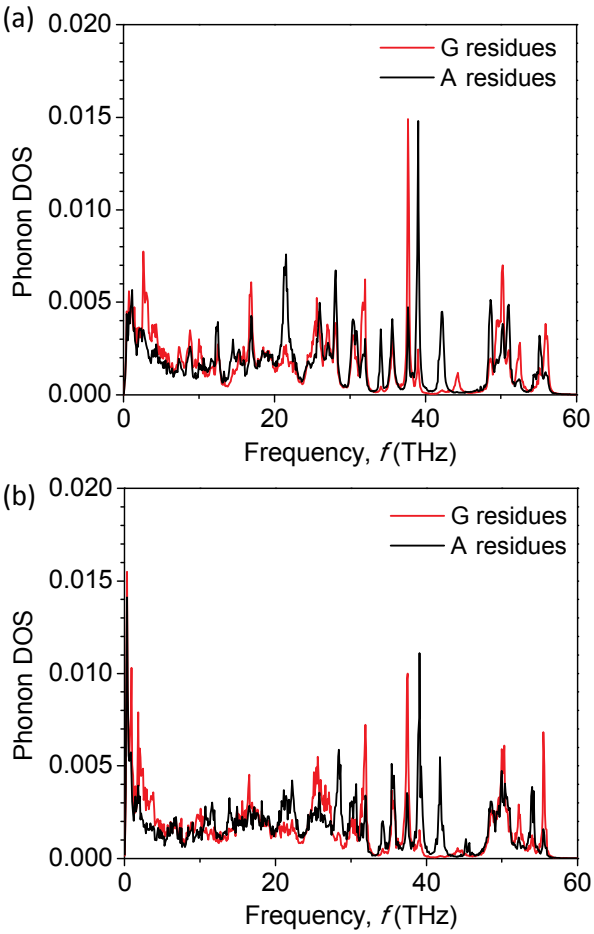

Figure 4. Partial phonon DOS projected on the glycine and alanine residues of (a) a GA8-5-1 β-sheet and (b) a standalone GA8-1-1 β-strand.

may engineer the side chains to change the effective area of the β-sheet. For example, the short side chains in the poly-G β-sheet can reduce the cross sectional area effectively, thereby increasing the thermal conductivity to the largest extent among the three types of β-sheet under investigation.

On the other hand, the poly-(GA) β-sheets are shown to have lower thermal conductivities than their counterparts with homogenous compositions (poly-A and poly-G). To understand how the heterogeneous composition affects thermal conduction, we have conducted phonon DOS (density of states) analysis on the poly-(GA) β-sheets. Figure 4*a* plots the partial phonon DOS of the GA8-5-1 β-sheet projected on the glycine and alanine residues, respectively. Very different phonon modes spanning from 0 to 60 THz are identified between the two types of residues. For example, the glycine residues are associated with unique peaks at 0.71, 2.71, 44.33, and 52.65THz, and have higher densities at 7.13, 8.96, 16.76, 31.85, 37.74, 50.23, and 55.86 THz; by comparison, the alanine residues show unique peaks at 1.18, 34.11, and 42.34THz, and have higher densities at 12.51, 21.44, 28.04, 38.78, and 49.02 THz. Based on these results, phonon dynamics is distinct in the glycine and alanine residues. When such phonons are carrying heat through the β-sheets, some of them may reflect back or experience mode conversion at the interfaces between the two different types of residues, dramatically decreasing the efficiency of thermal conduction. This is analogous to that in in superlattice nanowires which are composed of alternating materials in a periodic pattern. Several investigations[26] have shown reduced thermal conductivities of superlattice nanowires compared with that of the constituting materials,[37] based on similar mechanisms.

We note that, despite the similarities, the β-sheets have several unique characteristics that differ them from the superlattice nanowires. First, superlattice nanowires feature alternating chemical elements along the length direction which form many interfaces between the materials. In β-sheets, however, the chemical composition of the main phonon transport pathway, i.e. the backbone, is the same for all residues; different types of residues are differed in their side chains, which impose strong influences on the transport of phonon through the backbone chains. Second, the thermal transport in β-sheets is further complicated by the unique hydrogen bonding interactions between the neighboring β-strands. Figure 4*b* plots the partial phonon DOS of the standalone GA8-1-1 β-strand projected on the glycine and alanine residues, respectively. The two types of residues show very different phonon modes. And more importantly, by comparing Figure 4*b* with Figure 4*a*, it is readily seen that the low-frequency phonon modes in β-sheets are widened and have blue-shifted frequencies, due to the inter-strand hydrogen bonds. Indeed, in the β-sheets with heterogeneous amino acid compositions, the effects of alternating residues and hydrogen bonds are coupled, which complicates the thermal transport phenomena.

All sequence effects shown above were discussed using monolayer β-sheets as the model material. It is unknown, whether or not the revealed sequence effects would hold when multiple β-sheets stack to form nanocrystals. To answer this question, we simulated several multilayer β-sheets with the poly-A and poly-(GA) sequences. The results demonstrate that the sequence of amino acids influences the monolayer and multilayer β-sheets in a similar way. Figure 5 plots the thermal conductivities of two monolayer β-sheets (i.e. A16-7-1 and GA8-7-1), and four multilayer nanocrystals (i.e. A16-7-3, GA8-7-5, A16-7-3, and GA8-7-5). The thermal conductivities of all poly-A β-sheets are about twice as high as that of their poly-(GA) counterparts. In other words, the sequence effects discussed earlier for monolayer β-sheets hold in multilayer β-sheets. Another important finding is that the thermal conductivities of the

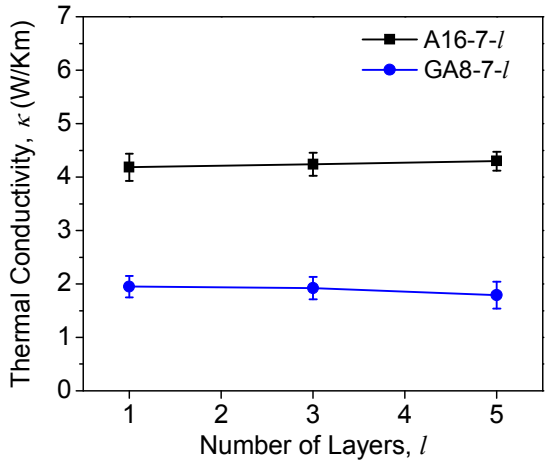

Figure 5. Thermal conductivity versus the number of layers in β-sheet structures with the poly-A and poly-(GA) sequences. Each layer has 7 β-strands and each strand has 16 residues.

poly-A (or poly-(GA)) β-sheets keep almost a constant as the number of layers varies. That means, the stacking of β-sheets does not change thermal conductivities significantly; phonon transport in the hydrogen-bonded β-sheets is not much influenced by the vdW interactions between the β-sheets.

The results shown in Figure 5 demonstrate that the thermal conductivities of the poly-A β-sheets (~4 $Wm^{-1}K^{-1}$) are higher than that of the poly-(GA) β-sheets (~2 $Wm^{-1}K^{-1}$). The sequence effects partly explain the different thermal conductivities between the *N. clavipes* dragline (~1.2 $Wm^{-1}K^{-1}$) and the *B. mori* silkworm silk (~0.54 $Wm^{-1}K^{-1}$), as the former silk has abundant poly-A β-sheets while the latter has rich poly-(GA) β-sheets. The differences between our simulation results and the experimentally measured values are mainly attributed to the complex compositions and structures of natural silks. As mentioned earlier, β-sheet nanocrystals only account for ~30% of the residues in the *N. clavipes* dragline, and ~50% in the *B. mori* silk. Moreover, each silk fiber is composed of multiple silk fibroins along with a skin layer and a periphery layer.[14] Therefore, in addition to the intrinsic thermal conductivities of the β-sheets, several other factors contribute to the overall thermal conductivities of the silks. These factors include the amorphous phase (most important), the interfaces between the amorphous and the β-sheet phases, water molecules, and the skin and core periphery materials. The influences of these factors, particularly the amorphous phase and its interfaces with β-sheet nanocrystals, may be a topic of future study.

Conclusions

To summarize, key molecular mechanisms underpinning the thermal conduction in three representative β-sheet types [i.e. poly-A, poly-(GA), and ploy-G] are studied to reveal the intrinsic effects of the amino acid sequence. With any of these sequences, β-sheets are shown to have thermal conductivities increasing with the number of β-strands, demonstrating the positive contributions of hydrogen bonds to heat transfer. At the same size, the poly-A β-sheet shows a thermal conductivity twofold higher than that of the corresponding poly-(GA) β-sheet, which partly explains why the *Nephila clavipes* dragline spider silk has higher thermal conductivity than the *Bombyx mori* silkworm cocoon silk. Moreover, the poly-G β-sheet shows the highest thermal conductivity among the three β-sheet types under investigation. All these sequence effects are caused by the distinct structures and unique phonon dynamics associated with the β-sheets. First, the alternating residues in the poly-(GA) β-sheets cause severe phonon mode mismatch across the G-A interfaces which obstruct thermal transport. Second, the β-sheets of homogeneous residues (i.e. poly-G and ploy-A) surprisingly demonstrate comparable thermal conductances despite the distinct thermal conductivities; the difference between their thermal conductivities is caused by the different cross-sectional areas which are tunable by side chain design. All these conclusions suggest that, by properly designing the amino acid sequence, protein β-sheets can be engineered to produce multifunctional synthetic silk and other biomaterials with tunable thermal properties.

Acknowledgements

The authors are grateful to the insightful discussions with Prof. Randolph V. Lewis, and the financial support by Utah State University.

References

1. C. L. Craig, *Annu Rev Entomol*, 1997, **42**, 231-267.
2. F. G. Omenetto and D. L. Kaplan, *Science*, 2010, **329**, 528-531.
3. Z. Z. Shao and F. Vollrath, *Nature*, 2002, **418**, 741-741.
4. Y. Shen, S. L. Redmond, J. M. Papadimitriou, B. M. Teh, S. Yan, Y. Wang, M. D. Atlas, R. J. Marano, M. H. Zheng and R. J. Dilley, *Biomed Mater*, 2014, **9**.
5. Y. Z. Wang, H. J. Kim, G. Vunjak-Novakovic and D. L. Kaplan, *Biomaterials*, 2006, **27**, 6064-6082.
6. G. H. Altman, F. Diaz, C. Jakuba, T. Calabro, R. L. Horan, J. S. Chen, H. Lu, J. Richmond and D. L. Kaplan, *Biomaterials*, 2003, **24**, 401-416.
7. L. Meinel, R. Fajardo, S. Hofmann, R. Langer, J. Chen, B. Snyder, G. Vunjak-Novakovic and D. Kaplan, *Bone*, 2005, **37**, 688-698.
8. A. Florczak, A. Mackiewicz and H. Dams-Kozlowska, *Biomacromolecules*, 2014, **15**, 2971-2981.
9. B. Subia, S. Chandra, S. Talukdar and S. C. Kundu, *Integrative Biology*, 2014, **6**, 203-214.
10. X. P. Huang, G. Q. Liu and X. W. Wang, *Adv Mater*, 2012, **24**, 1482-1486.
11. C. Xing, T. Munro, B. White, H. Ban, C. G. Copeland and R. V. Lewis, *Polymer*, 2014, **55**, 4226-4231.
12. G. Q. Liu, X. P. Huang, Y. J. Wang, Y. Q. Zhang and X. W. Wang, *Soft Matter*, 2012, **8**, 9792-9799.
13. J. Zhang, R. Rajkhowa, J. L. Li, X. Y. Liu and X. G. Wang, *Mater Design*, 2013, **49**, 842-849.
14. T. Lefèvre, M.-E. Rousseau and M. Pézolet, *Biophys J*, 2007, **92**, 2885-2895.
15. L. Zhang, T. Chen, H. Ban and L. Liu, *Nanoscale*, 2014, **6**, 7786-7791.
16. B. M. Foley, C. S. Gorham, J. C. Duda, R. Cheaito, C. J. Szwejkowski, C. Constantin, B. Kaehr and P. E. Hopkins, *The Journal of Physical Chemistry Letters*, 2014, **5**, 1077-1082.
17. J. D. van Beek, S. Hess, F. Vollrath and B. H. Meier, *Proceedings of the National Academy of Sciences*, 2002, **99**, 10266-10271.
18. S. B. Xiao, W. Stacklies, M. Cetinkaya, B. Markert and F. Grater, *Biophys J*, 2009, **96**, 3997-4005.
19. B. An, J. E. Jenkins, S. Sampath, G. P. Holland, M. Hinman, J. L. Yarger and R. Lewis, *Biomacromolecules*, 2012, **13**, 3938-3948.
20. A. Lazaris, S. Arcidiacono, Y. Huang, J. F. Zhou, F. Duguay, N. Chretien, E. A. Welsh, J. W. Soares and C. N. Karatzas, *Science*, 2002, **295**, 472-476.
21. C. Riekel, C. Bränden, C. Craig, C. Ferrero, F. Heidelbach and M. Müller, *Int J Biol Macromol*, 1999, **24**, 179-186.
22. F. Lucas, J. T. B. Shaw and S. G. Smith, *Nature*, 1956, **178**, 861-861.
23. J. Liu and R. G. Yang, *Phys Rev B*, 2010, **81**.
24. C. W. Padgett and D. W. Brenner, *Nano Lett*, 2004, **4**, 1051-1053.
25. R. Q. Pan, Z. J. Xu, Z. Y. Zhu and Z. X. Wang, *Nanotechnology*, 2007, **18**.
26. M. Hu and D. Poulikakos, *Nano Lett*, 2012, **12**, 5487-5494.
27. T. A. Blackledge, C. Boutry, S.-C. Wong, A. Baji, A. Dhinojwala, V. Sahni and I. Agnarsson, *Journal of Experimental Biology*, 2009, **212**, 1981-1989.
28. P. M. Cunniff, S. A. Fossey, M. A. Auerbach, J. W. Song, D. L. Kaplan, W. W. Adams, R. K. Eby, D. Mahoney and D. L. Vezie, *Polym Advan Technol*, 1994, **5**, 401-410.
29. F. Muller-Plathe, *J Chem Phys*, 1997, **106**, 6082-6085.
30. E. A. Algaer and F. Müller-Plathe, *Soft Materials*, 2011, **10**, 42-80.

31. P. K. Schelling, S. R. Phillpot and P. Keblinski, *Physical Review B*, 2002, **65**, 144306.
32. C. Nieto-Draghi and J. B. Avalos, *Mol Phys*, 2003, **101**, 2303-2307.
33. S. Plimpton, *J Comput Phys*, 1995, **117**, 1-19.
34. A. D. MacKerell, D. Bashford, M. Bellott, R. L. Dunbrack, J. D. Evanseck, M. J. Field, S. Fischer, J. Gao, H. Guo, S. Ha, D. Joseph-McCarthy, L. Kuchnir, K. Kuczera, F. T. K. Lau, C. Mattos, S. Michnick, T. Ngo, D. T. Nguyen, B. Prodhom, W. E. Reiher, B. Roux, M. Schlenkrich, J. C. Smith, R. Stote, J. Straub, M. Watanabe, J. Wiorkiewicz-Kuczera, D. Yin and M. Karplus, *J Phys Chem B*, 1998, **102**, 3586-3616.
35. D. Paschek and A. E. Garcia, *Phys Rev Lett*, 2004, **93**, 238105.
36. G. Miño, R. Barriga and G. Gutierrez, *The Journal of Physical Chemistry B*, 2014, **118**, 10025-10034.
37. X. B. Li and R. G. Yang, *Phys Rev B*, 2012, **86**.